COO-2218-201

CONF-810415--5

# FINITE-ORBIT METHOD FOR DYNAMIC ANALYSIS OF MIRROR FUSION SYSTEMS

MASTER

M. M. Campbell and G. H. Miley
Fusion Studies Laboratory
Nuclear Engineering Program
University of Illinois
Urbana, Illinois 61801 USA

A model (FOREMD) is described which treats plasma buildup in small mirror fusion devices where finite gyroradius effects are important to the dynamic evolution of the density and energy profiles. An energy-dependent group technique is employed, but unlike conventional point-kinetic diffusion models, the local density is calculated by a summing over orbits passing through the volume of interest. This treatment is particularly important during buildup via neutral beam injection where charge-exchange losses near the surface affect the inner-volume density distribution through loss of large orbit ions. As an example of the use of FOREMD, buildup processes in two experimental devices (2X-IIB and TMX) are examined.

DISCLAIMER

This report was prepared as an account of work sponsored by an agency of the United States Government. Neither the United States Government nor any agency thereof, nor any of their employees, makes any warranty, express or implied, or assumes any legal liability or responsibility for the accuracy, completeness, or usefulness of any information, apparatus, product, or process disclosed, or represents that its use would not infringe privately owned rights. Reference herein to any specific commercial product, process, or service by trade name, trademark, manufacturer, or otherwise, does not necessarily constitute or imply its endorsement, recommendation, or favoring by the United States Government or any agency thereof. The views and opinions of authors expressed herein do not necessarily state or reflect those of the United States Government or any agency thereof.

DISTRIBUTION OF THIS DOCUMENT IS UNLIMITED

JHS

# FINITE-ORBIT METHOD FOR DYNAMIC ANALYSIS OF MIRROR FUSION SYSTEMS

## INTRODUCTION

A finite-orbit technique to simulate plasma buildup in mirror fusion devices has been developed at UIUC and will be described here. In a small, hot, magnetically confined plasma, the ion orbit radius ($\rho_i$) can be comparable to the plasma radius ($R_p$). In a mirror-confined plasma where $S \equiv R_p/\rho_i \lesssim 20$ [e.g., in the 2X-IIB device[1] at the Lawrence Livermore National Laboratory (LLNL), $S \sim 3$], a "point-kinetic" treatment of ion interactions becomes inaccurate and a finite gyro-radius (FGR) model must be used. This is particularly important for treating losses due to cold-gas charge-exchange (c-x) near the plasma surface, since an energetic ion lost across the vacuum interface may have contributed to the density as far as $2\rho_i$ radially inward (Fig. 1A). A similar FGR effect applies to beam-deposited ions whose large orbits influence the density up to $2\rho_i$ from their trapping point (Fig. 1B). The deposition of orbit centers depends on the direction of $\vec{v} \times \vec{B}$. The necessity of using an FGR treatment in small plasmas has already been demonstrated by the authors and others.[2,3]

Important FGR effects such as those already discussed are considered in a dynamic computer model called FOREMD† described here. Unlike earlier finite-orbit models,[3,4] FOREMD is fully energy dependent and includes a quasi-linear treatment for the Drift Cyclotron Loss Cone (DCLC) instability.[5] Also included are effects of the local magnetic-field on ion orbits and a detailed accounting of possible charge-exchange reactions due to cold gas neutrals ($D_2^o$ and $D^o$) present in the vacuum chamber from neutral beam injector leakage, wall reflux and gas-box DCLC stabilization.

## DESCRIPTION OF THE TECHNIQUE

The FOREMD code solves a set of coupled, nonlinear, first-order differential equations that express the particle and energy balances in the plasma as a function of time and radial position. These equations are iterated in a finite-difference, explicit time-dependent form. An energy group approach is employed for the ion distribution while spatial effects are treated in cyclindrical coordinates using a finite ring mesh.

A flow diagram for FOREMD is shown in Figure 2A. The ions are tracked both as a density of orbit centers (DOC) and a time-averaged local density (TAD). The TAD is found from the DOC by summing contributions to each radial region (shell) made by ions with orbits traversing the

---

†Finite Orbit, Radial, Energy and Magnetic-field Dependence.

region (see Fig. 1B). The TAD is calculated at each energy to form a local distribution function corresponding to the energy grid used for the DOC distribution.

Actual contributions to a shell depend on orbit radius, the location of the orbit center and the DOC profile. The DOC profile in the present model is assumed to be uniform in a radial shell, making the radial profile a "histogram." The number of particles occupying a small annulus of thickness $\Delta R$ is just DOC x $2\pi R\Delta R$. The local TAD contribution is proportional to the orbit-fraction contained within the local shell ($\ell$) times the number of particles in the contributing shell (k) divided by the volume of the local shell, or:

$$n_i(E_i,R_\ell) \equiv TAD_{\ell i} = \sum_k f_{k\ell}\ DOC_k\ V_k/V_\ell\Big|_{E_i} \quad , \tag{1}$$

with the sum being over all contributing k and the terms being defined in the nomenclature section following the references.

The location of an orbit center is assumed to remain within the "birth" shell unless the DCLC instability is strong enough to cause the radial diffusion time to be comparable to the axial loss time, in which case cross-field diffusion of orbit centers is included. Slowing-down anisotropies over an orbit are ignores due to the long time scale and second-order nature of this effect. Radial diffusion of ions tends to be dominated by charge-exchange processes and DCLC diffusion in mirrors such as 2X and TMX.[6]

The orbit radius depends on both particle energy and the local magnetic field strength ($\rho \sim \frac{\sqrt{E}}{B}$). The present model calculates an average orbital radius from the energy and an average B over the orbit (approximated using a Taylor's expansion about the orbit center). Provision has also been made for treating slightly noncircular orbits, but results presented here do not include this effect because ion orbits are nearly circular for these relatively low-$\beta$ cases.

Ions with small orbits and those with energies well below the plasma potential ($q\phi p$) which are rapidly lost are not treated as having finite orbits. Such ions contribute to the local density or hardly at all, in the latter case. An arbitrary cutoff of ~ 0.1 times the average injection energy is usually used in FOREMD, less if the cutoff $\rho$ is not less than the radial shell thickness ($\Delta R$). In the present version, an error of 1% (noncumulative) was deemed acceptable for the density and beam trapping calculations (uncertainty in reaction cross sections introduce a much larger error in any plasma simulation). Therefore, several 2-digit orbit fractions (f) are encoded into one floating-point word along with additional information to identify which radial shells receive density contributions (see Fig. 2B). Ions whose orbits extend beyond the radial mesh (maximum R) are assumed to be lost (to a wall or limiter).

Once the lookups are used to calculate the TAD in a given shell, this density is then used in the ion Fokker-Planck treatment and to calculate all reaction rates ($n^2\langle\sigma v\rangle$) used in the balance equations discussed below.

## ION BALANCE EQUATIONS

The actual equations are set up in matrices, but the basic balances correspond to the following (for the local time-averaged density without a cold stream plasma). For ions:

PARTICLE BALANCE:

$$\text{ith group: } \frac{dn_i(E_i,R_\ell)}{dt} = \sum_k^{k_{max}} \frac{I_B(E_i,R_k)}{F(R_\ell)} (1 - \exp(-\Delta R/\Lambda_{tBi}))f_{k\ell} -$$

$$\sum_k^{k_{max}} f_{k\ell} \sum_j \frac{I_B(E_j,R_k)}{V(R_\ell)} (1 - \exp(-\Delta R/\Lambda_{tBij\ell}))\frac{\sigma_{cxB_{jk}}}{\sigma_{tBjk}} +$$

[Secondary Retrapping (gains-losses)] -

$$\frac{I_c(R_\ell)}{V(R_\ell)} (1 - \exp)-\Delta R/\Lambda_{tc\ell})) \frac{\sigma_{cxc_\ell}}{\sigma_{tc_\ell}} -$$

$$n_i(R_\ell)\left[\sum_j \frac{n_j}{\tau_{ij}} P_{LC_{i\ell}} - \sum_j n_j \langle\sigma v\rangle_{F_{ij\ell}}\right], \text{ and} \qquad (2)$$

ENERGY BALANCE:

$$\frac{dn_iE_i}{dt} = E_i \left.\frac{dn_i}{dt}\right|_{R_\ell} - (E_i - E_e) \left.\frac{n_in_e}{\tau_{ie}}\right|_{R_\ell}, \qquad (3)$$

where $\frac{dn_i}{dt}$ is given in Eqn. 2 and other terms used are defined in the nomenclature at the end of this article.

The ion particle balance determines the rate of change of the local density for the ith energy group ($n_i$) at the $\ell$th radial position ($R_\ell$) to the various sources and loses at the kth radial position. The terms to the right, in order of appearance, are the neutral beam trapping rate, beam c-x loss (includes DCLC), and loss of fuel ions due to fusion.

The ion energy balance accounts for changes associated with ion losses and energy exchange with background electrons. Thus the rate-of-change of nE, the density-energy product, is determined by the particle loss-rate for each energy group times the energy of that group minus the energy loss rate due to electron drag. The electron energy transfer rate is calculated using Sivukhin's[7] formulations which are satisfactorily accurate and faster to calculate than a multispecies Fokker-Planck treatment. Spreading of the ion distribution is calculated by a Fokker-Planck treatment which is formulated to conserve particles and energy

(to within 1 part in $10^7$), all plasma losses being calculated external to this relaxation as already described above.

Gains and losses for the TAD distribution are converted via a matrix inversion to a change in the DOC at the end of each timestep. The new DOC is then used to calculate the TAD for the next timestep.

## ELECTRON BALANCE EQUATIONS

The electrons, because of their small gyroradii and rapid self-equilibration are treated with a conventional fluid theory. Thus their particle and energy balances are (for the $\ell$th shell):

PARTICLE BALANCE:

$$\frac{dn_e}{dt} = -\left(\frac{dn_e}{dt}\right)_{LC_\ell} + \sum_j I_B(E_j,R_\ell)(1-\exp(-\Delta R/\Lambda_{tj\ell}).\left(\frac{\sigma_{ion_{j\ell}}}{\sigma_{tj\ell}}\right)$$

$$+ \frac{I_c(R_\ell)}{V(R_\ell)}(1 - \exp(-\Delta R/\Lambda_{tc\ell})).\left(\frac{\sigma_{ion_{c\ell}}}{\sigma_{tj\ell}}\right) \quad \text{and} \tag{4a}$$

$$\left(\frac{dn_e}{dt}\right)_{LC} = 3.9\text{x}10^{-15}\, n_e^2\, \phi_p^{-3/2}[2(\tfrac{x}{\pi})^{1/2} \exp(-x) + \text{erfc}\,(x^{1/2})] \tag{4b}$$

$$\text{where } x \equiv \frac{q\phi_p}{\frac{1}{2}m_e v_e^2}\ , \text{ (Ref. 8);} \tag{4c}$$

ELECTRON ENERGY:

$$\frac{dn_e E_e}{dt} = -(\tfrac{2}{3} + q\phi_p)\left(\frac{dn_e}{dt}\right)_{LC_\ell} + \sum_j (E_j - E_e)\left.\frac{n_i n_e}{\tau_{ie}}\right|_{R_\ell} +$$

$$\frac{m_e}{m_{ion}} \sum_j I_B\,(E_j,R_\ell)\, E_j\,(1-\exp(-\Delta R/\Lambda_{tj\ell})).\left(\frac{\sigma_{ion_{j\ell}}}{\sigma_{tBj\ell}}\right) . \tag{5}$$

The electron density buildup rate is balanced by the loss-cone loss and the beam and cold-gas ionization contributions, respectively, on the right in Eqn. 4a. The electron energy loss-rate is a balance between the loss-cone loss, which removes an energy $q\phi_p + T_e$ in crossing the plasma potential ($\phi_p$) barrier, and the energy gained from the ions, with the third term on the right of Eqn. 5, the ionized-beam contribution, being very small.

## MODEL TESTING

Various tests were run to determine that FOREMD worked properly. In addition to checking the energy and particle balances and solution convergence for the radial and energy mashes, a comparison with a similar model under development by A. Futch at LLNL was performed.[9] The radial density profile comparison is shown in Fig. 3 for the case of 200-A, 18-keV injection into a 2-keV, $2.5 \times 10^{13} cm^{-3}$ density target. The FOREMD model (labeled M.C. in the fiture) used a step-profile radial target density while the Futch model initialized the target with a parabolic profile. Good agreement is observed with the parabolic target bracketed by the 8-cm and 10-cm target FOREMD results. The temperature profiles also showed good agreement. Later comparisons of FOREMD predictions for 2X-IIB with the experimental results also showed good agreement.

## ILLUSTRATIVE APPLICATIONS

The FOREMD model has been used to study plasma buildup in the previously operating 2X-IIB mirror and the mirror end plugs of the present TMX experiment at LLNL. Some results are briefly outlined here.

Parameters employed for the 2X-IIB target plasma are given in Table I. For 2X studies, the ion distribution ranged in energy from 5 eV to 100 keV using 38 energy groups and the radial grid consisted of 40 shells of thickness 0.5 cm each. A result illustrating the importance of charge-exchange erosion is shown in Fig. 4. Here a high-energy (18 keV) neutral-beam of 375 A equivalent is injected into the target plasma at time t = 0 in order to heat and buildup the plasma. To simulate the cold gas that simultaneously enters the vacuum chamber through the injector beam lines and gas-box leakage, an additional low-energy stream of neutrals equivalent to ~ 50 A is included. Charge-exchange reactions between these cold neutrals and plasma ions create a hot neutral, which can escape, and a cold ion, which is rapidly accelerated into the loss cone by the plasma potential. Indeed, as seen from Fig. 4, the resulting losses are so great that, despite an early rise in the center-line density, the plasma is destroyed after ~ 1-1/2 ms. A similar run, but with 450-A beam injection, achieves buildup. Such charge-exchange plasma quenching has been observed in LLNL experimental runs under adverse vacuum conditions.[6]

The previous results omitted DCLC effects for simplicity. With DCLC losses minimized by a stabilizing cold plasma stream, c-x erosion remains a very important effect.

Figures 5A and B show a FOREMD simulation of a 2X-like plasma for injection of 600 A at 14 keV (to simulate a multi-energy component beam) into a ~ 2-keV target of density $5 \times 10^{13}$ $cm^{-3}$ and a total, penetrating stream current of about 150 A. The density decays until a near-equilibrium is reached at t ~ 0.6 ms and a mean density of about $3.5 \times 10^{13}$ $cm^{-3}$. The central "dip" is due primarily to c-x effects. The ion temperature evolution is shown in Fig. 5B and equilibrium is reached in about a c-x displacement time. The temperature rise near the plasma edge during buildup is a result of trapped, hot beam ions whose orbits extend out into the target/vacuum interface region. Near equilibrium, $W_i (\sim T_i)$ approaches an average 12.5 keV and $W_e$ approaches ~260 eV ($T_e$ ~ 170 eV). This result agrees fairly well with that obtained by Berk for a similar 2X case using a global DCLC treatment (within 30% in both density and

temperature without taking into account any differences between models).[5]

The ion energy distribution for this 2X-like case is shown in Fig. 5C at time t=0.4 ms and radius R=2.5 cm. The low-energy peak occurs at the stream energy. The distribution falls rapidly from this energy and begins to rise for particle energies above the plasma potential energy ($q\phi_p$). Above energy ($q\phi_p$) the amplitude rises rapidly and levels off as the target energy ($W_T$) is approached. The flat region around this point is primarily the target remnant which is being slowly displaced by beam ions. A second peak occurs at the injection energy ($E_{inj}$) as expected. Superimposed on this peak is Riviere's[10] numerical fit of the Fokker-Planck mirror distribution which would be generated for 14-keV injection in the classical (no DCLC or stream) case. In the DCLC/stream case, electron drag rapidly pulls hot ions down in energy until the critical loss energy ($q\phi_p$) is reached and the ions escape. [The high energy "tail" of this distribution requires about one ion-ion collision time (~3 ms) to fill out completely.]

Figure 6 shows a comparison of plasma boundary density profiles for cases with and without incident cold gas (the interior profile is unaffected at such high plasma densities with 14-keV injection and is not shown). This case is essentially identical to that of Fig. 5A. Boundary erosion has steepened the density profile in the case with 50 A of $D^\circ$ incident, indicating the strong effect of c-x losses in this region. A case (not shown) run with 65-A $D^\circ$, instead of 50-A, decays to extinction in about 2 ms, similar to the case illustrated in Fig. 4.

## BUILDUP IN TMX END CELL

Buildup in the TMX end cell (one of two conventional mirrors used to electrostatically stopper the ends of a long solenoidal region whose effects are presently ignored) for 14- to 20-keV injection yields a plasma essentially identical to 2X (particularly for 2X operated at high $\vec{B}$). Therefore, simulations were done for cases with 40-keV injection (soon to come on line) into a target built up by the 20-keV injections ($W_i \sim 15$ keV, $W_e \sim 350$ eV, $n \sim 5\times10^{13}$).[11]

As in the 2X case, charge-exchange erosion can be an important plasma loss mechanism. Although the c-x cross section is lower at 40 keV than at 20 keV, the TMX 40-keV beam current is lower than in the 2X, 20-keV case. Also the trapping mean-free-path ($\Lambda_t$) is longer and electron ionization of $D^\circ$ is less at this higher energy.

The plasma density evolution was again calculated for a 50-A incident $D^\circ$ case with 100-A injection into the target already described. The density profile evolution is shown in Fig. 7. For this low injection current the initial density of $5\times10^{13}$ cm$^{-3}$ is too small for a c-x equilibrium to occur and the plasma eventually decays away (beam trapping is already < 30 A by t = 1.4 ms). This run therefore, verifies the importance of c-x losses in 40-keV TMX buildup. Further studies have shown that at least 160 A of injection is required to overcome the c-x erosion due to 50-A $D^\circ$ gas.

## CONCLUSION

Examination of these and related results has lead to two important conclusions. First, it is found that for successful buildup charge-exchange erosion must be overcome before the cold gas penetrates to the plasma core. Second, c-x erosion can inhibit and even stop plasma buildup in both 2X and the 40-keV TMX.

The FOREMD code represents a unique combination of a Fokker-Planck energy treatment and discrete orbit physics which is necessary to describe the plasma in small systems where $S \lesssim 20$. Application of this technique to studies of plasma buildup in mirror devices such as 2X-IIB and TMX have provided new insights into key erosion mechanisms such as charge-exchange and had lead to suggested improvements in neutral-beam injection techniques.

## REFERENCES


[1] F. H. Coensgen, Lawrence Livermore Laboratory Report LLL-Prop-148, Jan. 1977.

[2] M. Campbell, Lawrence Livermore Laboratory Report UCID-17458, May 1977.

[3] B. Stallard, Lawrence Livermore Laboratory Report UCRL-51784, March 1975.

[4] A. H. Futch, et al., Plasma Phys., 14, 211 (1972).

[5] H. L. Berk and J. J. Stewart, Lawrence Livermore Laboratory Report UCRL-78407, 1976.

[6] A. Futch, Lawrence Livermore Laboratory, private communication, summer 1980.

[7] D. V. Sivukhin, Reviews of Plasma Physics, 4, 93 (1966).

[8] T. J. Dolan, et al., Lawrence Livermore Report UCID-17576, 1977.

[9] A. Futch, Lawrence Livermore Laboratory, private communication, fall 1979.

[10] A. C. Riviere, Nuclear Fusion, 11, 363 (1971).

[11] F. H. Coensgen, Lawrence Livermore Laboratory Report LLL-PROP-142, March 1976.

## NOMENCLATURE

| | |
|---|---|
| $n$ | density |
| $E$ | energy |
| $V$ | volume of radial shell |
| $\Delta R$ | thickness of radial shell |
| $R$ | radius |
| $I$ | current |
| $\sigma$ | cross section |
| $\phi_p$ | plasma potential |
| $P_{LC}$ | loss-cone probability |
| $\Lambda$ | mean free path |
| $\tau$ | collision time/(particles/cm$^3$) |
| $m$ | mass |
| $q$ | electron charge |
| $f$ | contributing orbit fraction |

Subscripts

| | |
|---|---|
| i,j | ith or jth energy group |
| B | beam |
| t | total |
| c | cold gas |
| cx | charge exchange |
| ion | ionization or ion |
| F | fusion |
| LC | loss cone |
| e | electron |
| k,ℓ | spatial grid point |

Table I. 2X-IIB Parameters

$\bar{E}_{ion} \sim 2.4$ keV

$E_c \sim 200$ eV

$n_{ion} \sim 8. \times 10^{12}$ cm$^{-3}$

$R \sim 8$ cm

$B \sim 1.0$ T

Figure 1a. Shows how a Large-Orbit ion (center at P) Contributes to the Density Over a Large Region of the Plasma (hashed area).

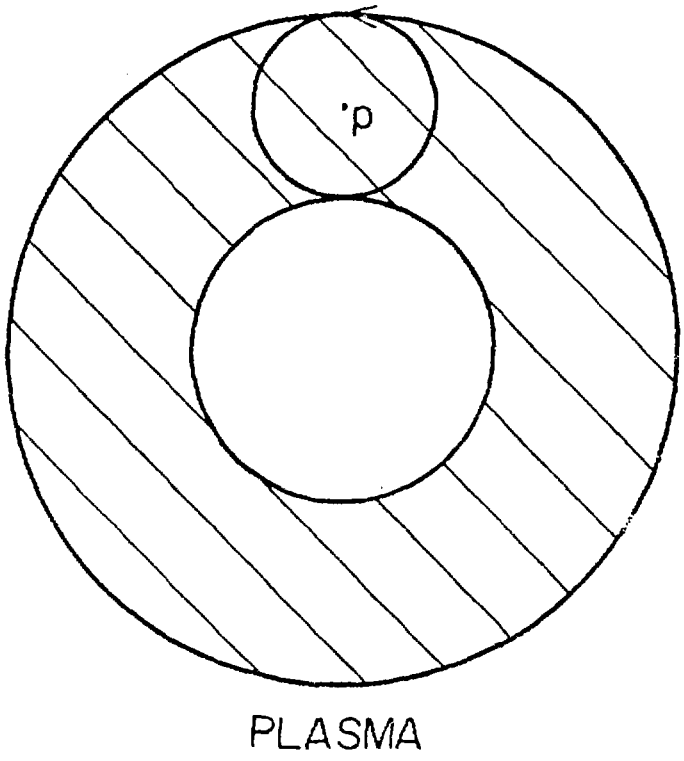

Figure 1b. Shows the Displacement of the Gyro-Center of a Trapped Beam Ion due to the $\vec{v}x\vec{B}$ Force. The orbit is tangent to the beam at the point of formation "x". Assuming uniform trapping and a constant $\rho_i$ over a small plasma region which intercepts the beam, the deposition of orbit centers is found by displacing the trapping region by $\rho_i$ and superimposing it back onto the original radial shell grid. Depending on the location of the beam and the direction of $\vec{v}x\vec{B}$, the orbit centers may be deposited either inward or outward radially.

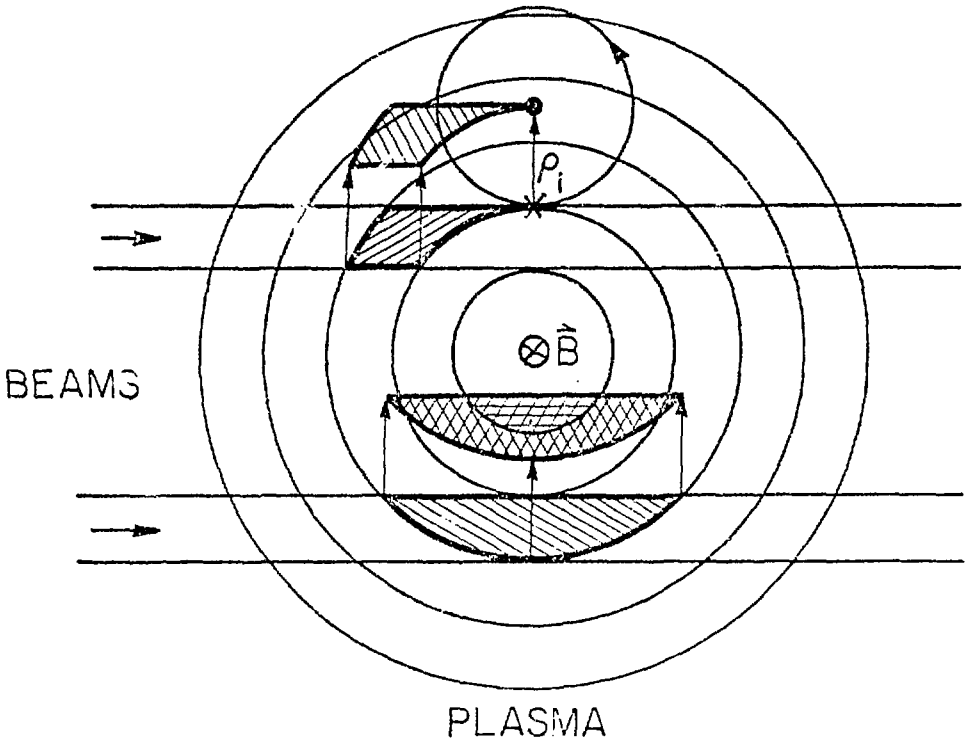

Figure 2A. Shows a Flow Chart of Processes in the Time-Dependent FOREMD Model. Depose and FOREMSET generate the beam deposition and density conversion lookups, respectively.

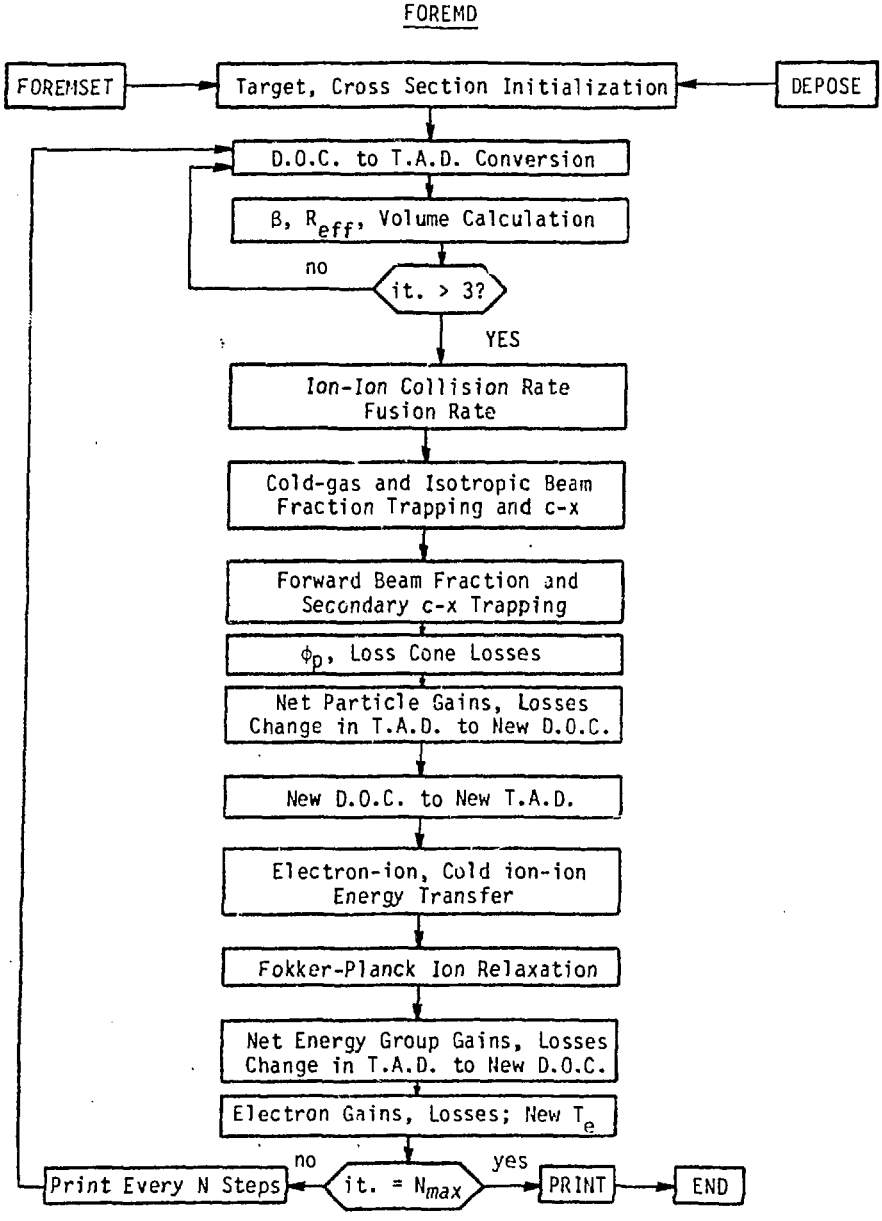

Figure 2B. Encoding of Density Transformation as 2 Digit (%) Orbit Fractions in a Word of Memory Capable of 15 Digit Accuracy. Up to 6 words per orbit can be used in the present model, allowing storage of ~ 34 contributions to different adjacent shells, sufficient for most applications. The sum of these percentage contributions is normalized to add up to 100 (%), as shown in the sample above. The first shell datum is a 3-digit number to accommodate a possible 100% contribution to a shell.

| | | | | | | | | | | | | | | |
|---|---|---|---|---|---|---|---|---|---|---|---|---|---|---|
| 1 | 5 | 1 | 8 | 0 | 0 | 3 | 2 | 8 | 5 | 4 | 1 | 5 | 0 | 0 |
| ↑ | | ↑ | | | ↑ | | ↑ | | ↑ | | ↑ | | ↑ | |
| 1st shell | | last shell | | | 15 | | 16 | | 17 | | 18 | | (5th shell) | |

Figure 3. Shows a Comparison Between Results From A. Futch's Code (A.F.) and the FOREMD Model (M.C.) Using two Different Targets. The Futch results are for a parabolic target density profile (8-cm half-max) and this is compared to FOREMD cases using 8-cm and 10-cm step-function (square) radial profiles. Excellent agreement is observed at time t=1 ms. Later tests show that the agreement remains very good for times of at least 10 ms.

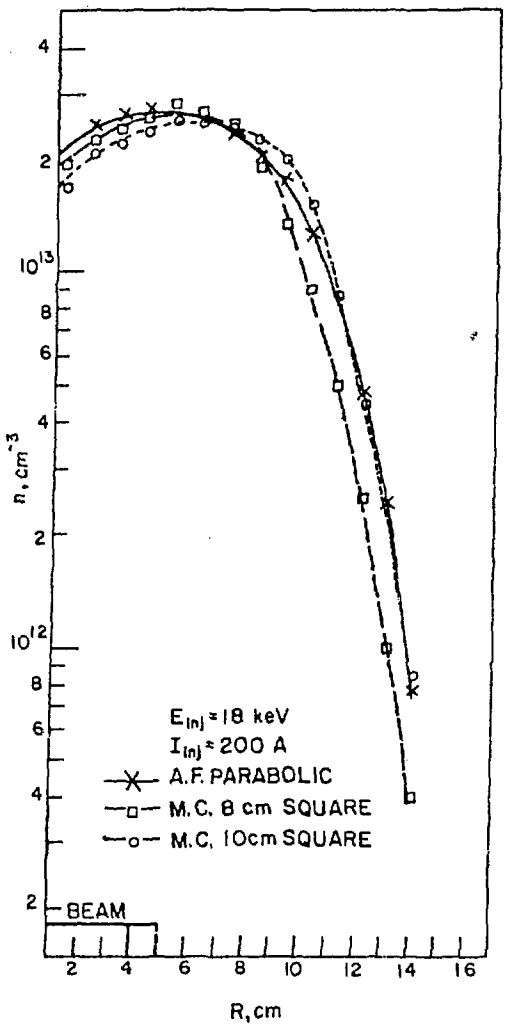

Figure 4. Shows the c-x Erosion (due to ~ 50-A D°) and Decay of a 2X-like Plasma Supported by 375 A of 18-keV Beam.

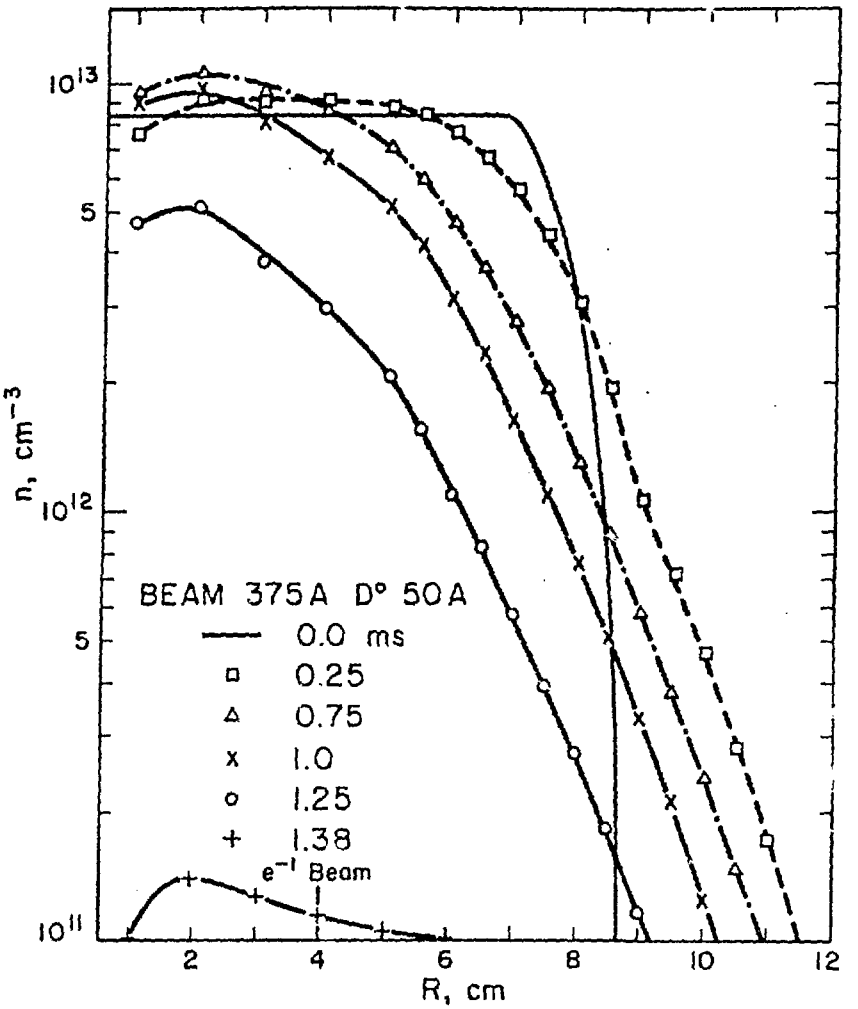

Figure 5A. Plasma "decay" to Near-Equilibrium (t ~ .4 ms) for a Stream Stabilized 2X-like Case with 600-A Injection at 14 keV and a Total Stream Current of 150 A Into a Dense Target ($W_{iT}$ = 2.4 keV, $n_T$ = $5 \times 10^{13}$ $cm^{-3}$). The central density "dip" is a result of beam attenuation.

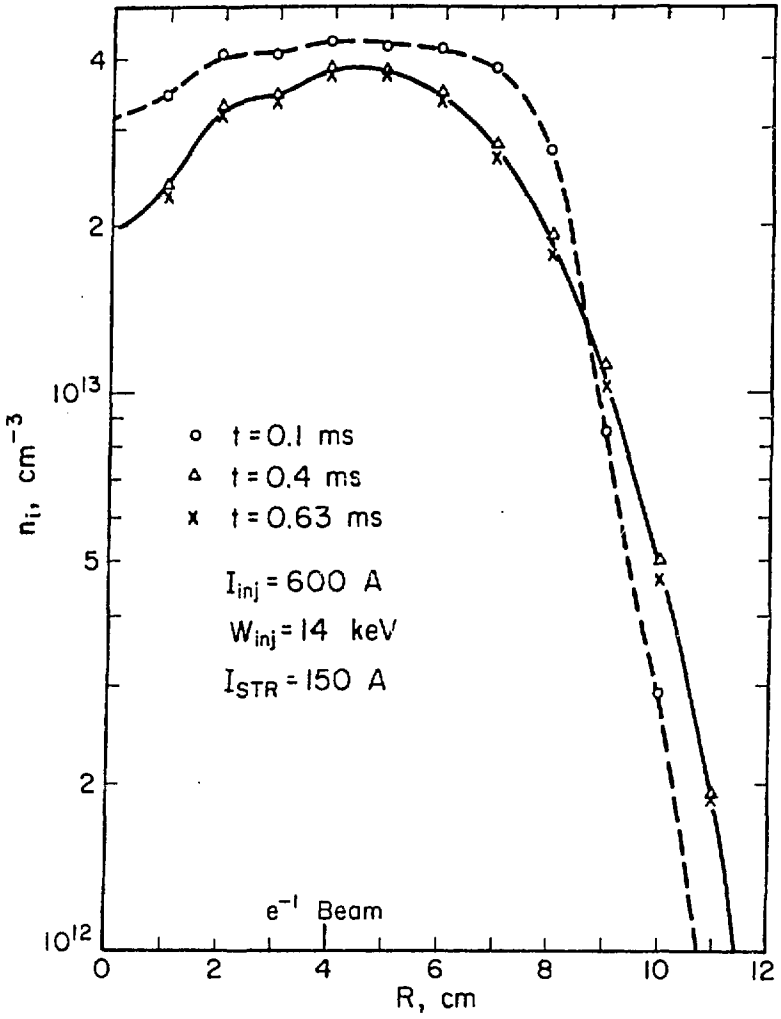

Figure 5B. Ion Temperature Evolution for Fig. 4A. The high temperature boundary at t = 0.1 ms is due to hot ion orbits extending into the near-vacuum region. Later c-x replacement of target ions raises the internal ion temperature.

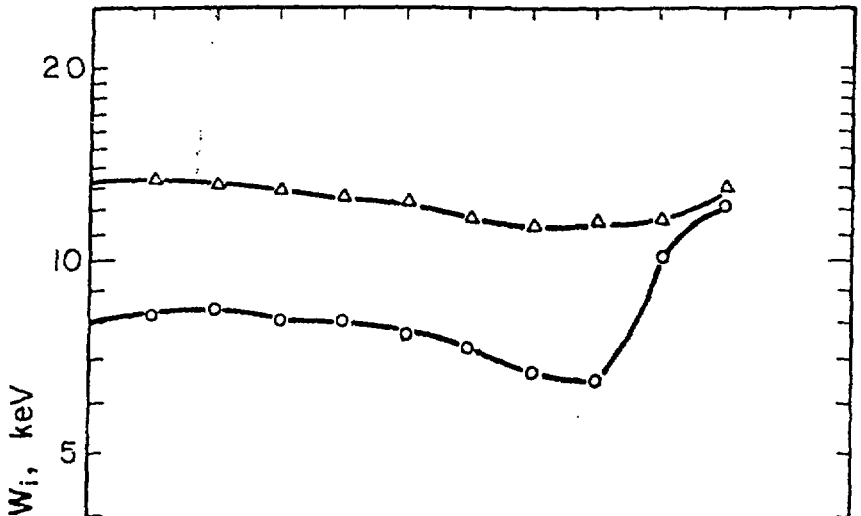

Figure 5C. The ion energy distribution, f(F), for Fig. 5A at t = 0.4 ms and at R = 2.5 cm. Peak occurred at the stream energy ($E_{STR}$) and injection energy ($E_{inj}$) with a remnant at the original target energy ($W_T$). The "valley" occurs below the potential energy due to loss-cone losses. For comparison, a fit to the classical 14-keV distribution (squares) is included.[10]

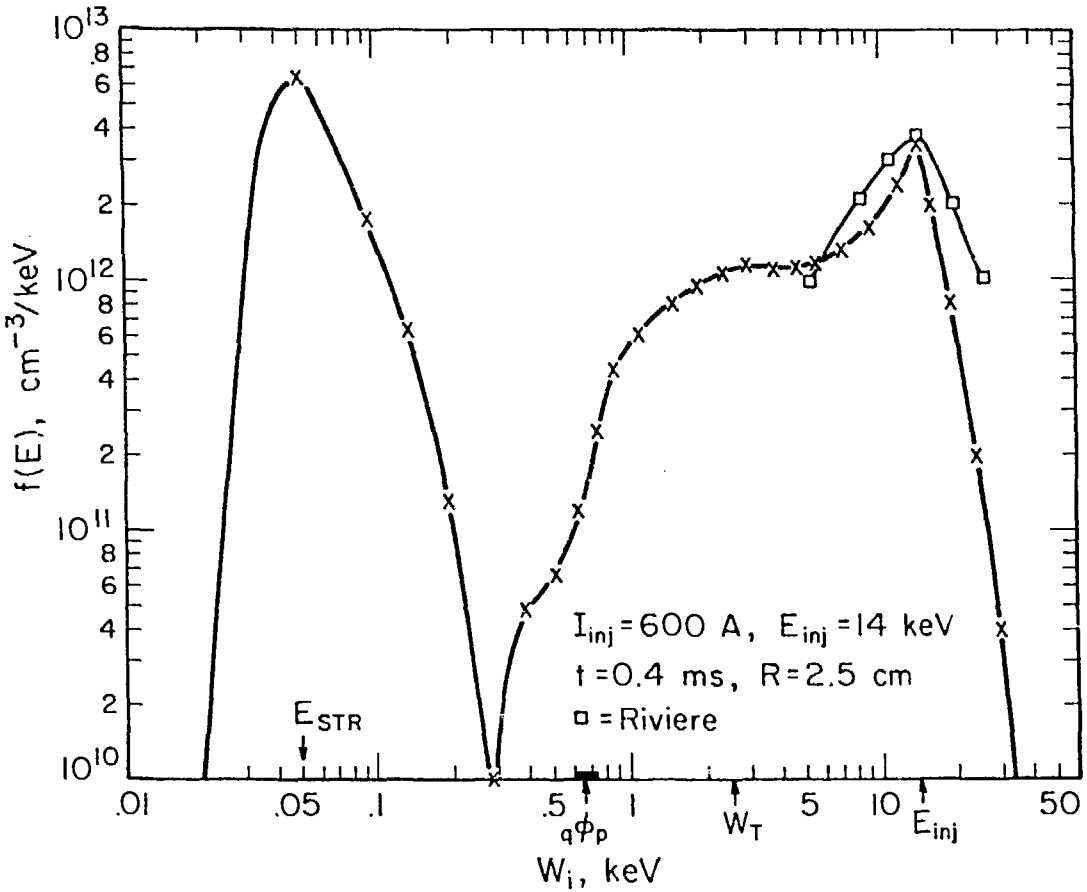

Figure 6. Edge Profiles for a 2X-like Plasma With Parameters Like That in Fig. 5A for Cases Both With (50-A) Cold gas and Without gas. The boundary profile steepens somewhat while the interior (R < 7-9 cm) is unaffected.

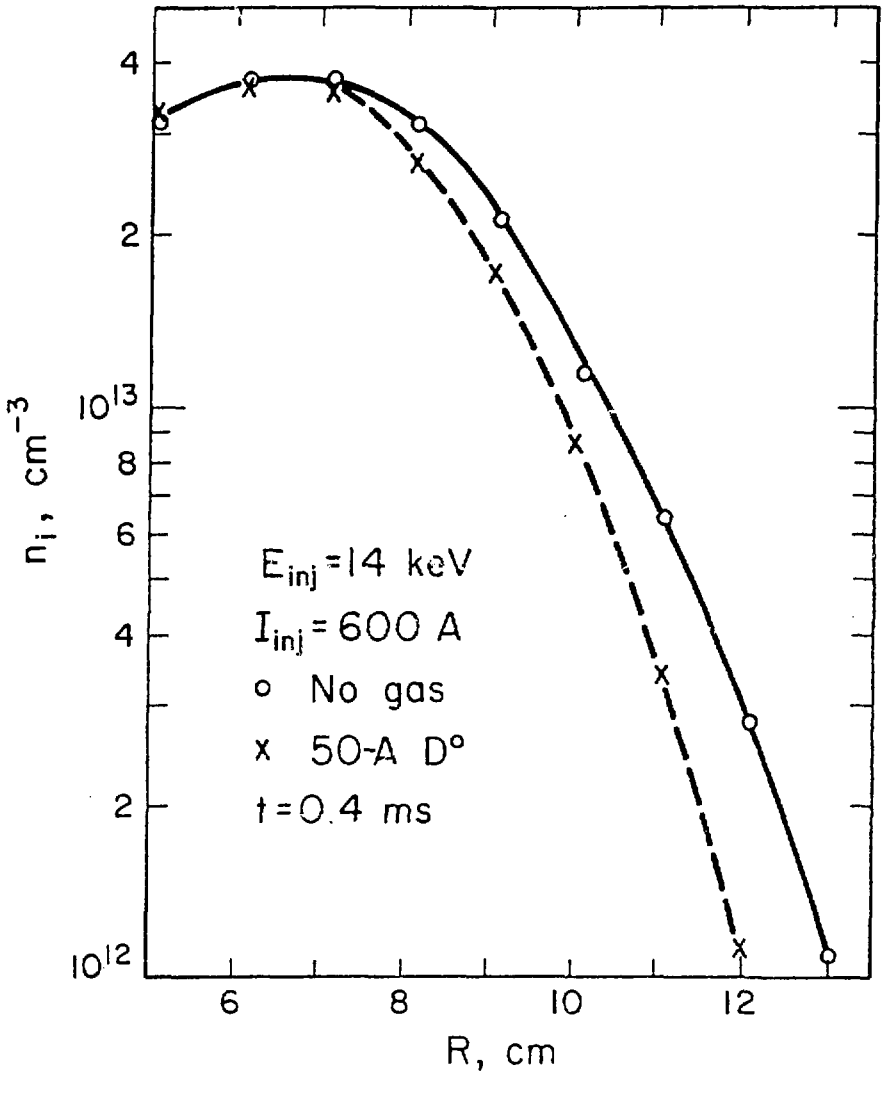
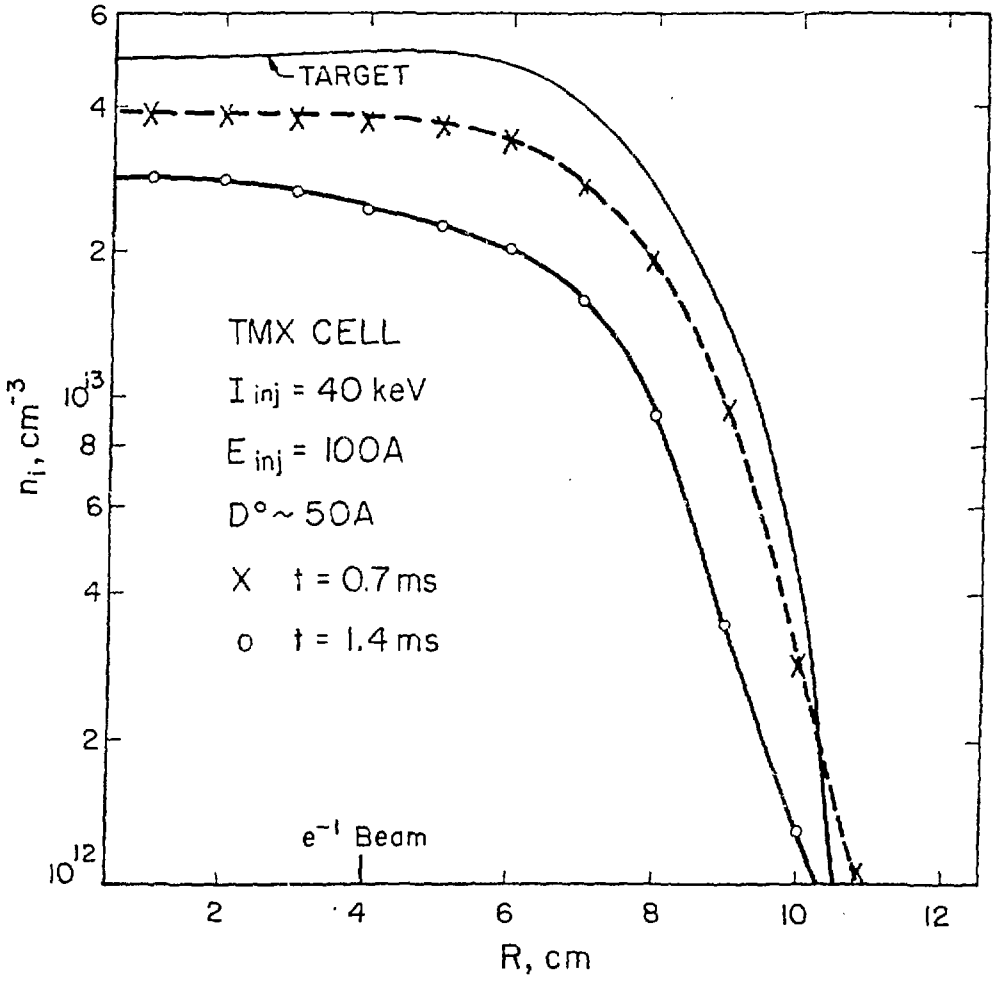
Figure 7. TMX End-Cell Case for 100-A Injection at 40 keV into a Target Described in the Text. The initial density of $5 \times 10^{13}$ $cm^{-3}$ is not sufficient to trap sufficient beam to replace cold e-x losses and the plasma eventually decays away.